Modified elastic model for viscosity in glass-forming systems

Siva Priya Jaccani, Ozgur Gulbiten, Douglas C. Allan, John C. Mauro, and Liping Huang

Phys. Rev. B **96**, 224201 — Published 7 December 2017

DOI: 10.1103/PhysRevB.96.224201

Modified elastic model for viscosity in glass-forming systems

Siva Priya Jaccani[1], Ozgur Gulbiten[2], Douglas C. Allan[2], John C. Mauro[3] and Liping Huang[1,*]

[1]*Department of Materials Science and Engineering, Rensselaer Polytechnic Institute, Troy, New York 12180, USA*

[2]*Science and Technology Division, Corning Incorporated, Corning, New York 14831, USA*

[3]*Department of Materials Science and Engineering, The Pennsylvania State University, University Park, Pennsylvania 16802, USA*

[*]*Corresponding author: huangL5@rpi.edu*

ABSTRACT

For most glass-forming liquids, the temperature dependence of viscosity is non-Arrhenius. Despite the technological and geological importance, the origin of this non-Arrhenius temperature dependence of viscosity remains elusive to date and constitutes an important but unsolved problem in condensed matter physics. It has become increasingly clear in recent years that high-temperature elasticity and viscosity of glass-forming liquids are strongly correlated. This work proposes a modified elastic model to predict equilibrium viscosity of glass-forming liquids. The new elastic model considers the configurational entropy as a factor controlling the activation energy for viscous flow in addition to the high-frequency shear modulus as in the Dyre shoving model. It works much better than the shoving model in fitting equilibrium viscosity for both strong and fragile systems. The new model also has the capability to estimate the non-equilibrium isostructural viscosity of glass from the equilibrium viscosity and the temperature-dependent elasticity of the glassy state.

KEYWORDS: Glass-forming liquids, non-Arrhenius behavior, viscosity-elasticity relationship, shoving model, Adam-Gibbs model, isostructural viscosity

I. INTRODUCTION

Each glass manufacturing operation — melting, fining, forming, and annealing — requires a certain well-defined shear viscosity range[1] and consequently a specific temperature range for that operation.[2] Hence, it can be said that industrial glass production is mostly governed by the temperature-dependent shear viscosity.[1,3] It is thus of great importance to have accurate knowledge of the scaling of viscosity with temperature, considering its super-Arrhenius rise as a melt is cooled toward the glass transition. Experimental measurement of viscosity is challenging for high temperature melts, and time consuming or even prohibitively expensive at low temperatures.[1,4,5] This has motivated great efforts in developing reliable viscosity models and in understanding the origin of the non-Arrhenius temperature dependence of viscosity in glass-forming liquids.[6]

The dynamic and thermodynamic origin of the non-Arrhenius temperature dependence of viscosity has been studied with great interest over the past century with no theory being accepted so far with consensus.[7] The two most influential atomistic models that have been proposed over the years to explain this phenomenon are the configurational entropy model[8] of Adam and Gibbs and the elastic shoving model[9] of Dyre et al.[7] While either model claims to work well alone to explain the temperature dependence of viscosity, some believe that both models are two sides of the same coin[7,10,11], and a recent study indicated the necessity to combine the two.[12] In this work, we argue that one model cannot be a replacement for the other and that both configurational entropy as well as elasticity influence viscosity and that both these factors together explain the non-Arrhenius nature of its temperature dependence.

The Dyre shoving model assumes that the activation barrier for viscous flow has two contributions[9]: (i) rearrangements of molecules or structural units, when a thermal fluctuation leads to extra space being created locally; (ii) 'shoving' aside the surrounding liquid to reduce the first contribution. According to the shoving model, the main contribution comes from (ii), i.e., the activation energy is mainly elastic energy. Furthermore, it is assumed that all flow events possess spherical symmetry, i.e., the surroundings are subject to a pure shear displacement and not associated with any density change. Since this displacement happens on a short time scale, the shoving work is proportional to the instantaneous shear modulus[13], which leads to the temperature-dependent shear viscosity

$$\eta(T) = \eta_\infty \exp\left[\frac{\mu_\infty(T) V_c}{k_B T}\right], \tag{1}$$

where $\eta(T)$ stands for viscosity at a temperature T, η_∞ is the viscosity at high temperature, k_B is Boltzmann's constant, $\mu_\infty(T)$ is the temperature-dependent instantaneous shear modulus[14,15] at T and V_c is a characteristic microscopic volume, assumed to be temperature-independent in the shoving model. Thus, according to the shoving model, the dynamics of the glass-forming liquid is completely controlled by elasticity through the instantaneous shear modulus.[4] Some limitations

of the shoving model are that it systematically underestimates the values of fragility[4] and that it was originally derived for the equilibrium regime only.

Apart from the viscosity of the glass forming melt, it is also very important to estimate the viscosity of the resultant glass. Phenomenological models for estimating the non-equilibrium viscosity as a function of temperature include Narayanaswamy[16], Mazurin[17], Avramov[18] and Mauro-Allan-Potuzak (MAP)[3] models, just to name a few. The limitations of these models are that they are empirical and that the model parameters lack a direct physical interpretation.[19] The MAP model was recently modified with physically-meaningful parameters.[19,20] The shoving model was previously extended to the non-equilibrium regime[21] by including the effect of thermal history according to

$$\ln\left(\frac{\eta\left(T,T_f\right)}{\eta_\infty}\right)=\frac{\mu_\infty(T,T_f)V_c}{k_BT}. \tag{2}$$

It was found that Eq.(2) yields a significantly smaller change in viscosity with fictive temperature compared to what is observed experimentally.[21] It was suggested that there are factors beyond the evolution of shear modulus such as configurational entropy that control the non-equilibrium viscosity of glass.[21]

In this work, we propose a modified elastic model for viscosity which is an improvement over the Dyre shoving model in the equilibrium regime. The new elastic model considers the influence of both configurational entropy and high-frequency shear modulus in controlling the activation energy for viscous flow. With the new model, using only equilibrium viscosity data along with glass elasticity, non-equilibrium isostructural viscosity can be estimated. This is particularly useful because elasticity of glass is much easier to measure than viscosity. Non-equilibrium isostructural viscosity predicted by the new model agrees very well with Yue's isostructural viscosity model[22] as well as Mazurin's experimental measurements on a standard NBS 710 glass.[17] The modified elastic model makes way for a better understanding of the roles that elasticity and configurational entropy play in controlling viscosity.

II. EXPERIMENTAL METHOD

Silicate glasses from different chemical systems were studied in this work and shown in Table 1. The procedure by which the first eight sodium aluminosilicate glasses containing CaO and/or MgO were synthesized can be found elsewhere.[4] Albite and diopside glasses were synthesized by the melt-quenching method and annealed near their respective glass transition temperatures for 1 hour before being cooled down in furnace to room temperature. NIST 710A was equilibrated and held isothermally for two minutes at 655 °C and then cooled at 50 °C/min (T_f= 564.4 °C) or at 0.2 °C/min (T_f= 516.9 °C) from the supercooled liquid to room temperature. The cathedral glass was rapidly quenched from 635 °C to room temperature after being held

isothermally for two minutes. Corning Jade® glass[3] was annealed at various fixed temperatures ($T_<T_f$) and then cooled slowly to room temperature. The thermal history of Corning EAGLE XG® glass[3] was set by the fusion draw process through which it was manufactured without annealing.[19] A modified version of the calorimetric area matching method[23] was used to determine fictive temperatures of the NIST 710A, cathedral glass, EAGLE XG, and Corning Jade glass. NBS 710 glass was annealed at 522 °C for 2 hours and then cooled at 50 °C/min to room temperature to match the thermal history of the glass samples used in Mazurin's experiments.[17] The fictive temperature of the NBS 710 glass sample so obtained is taken as 522 °C. For albite, diopside, the eight sodium aluminosilicate glasses containing CaO and/or MgO, the glass transition temperature (T_g) was taken as the fictive temperature after annealing. Here, T_g is the temperature corresponding to a viscosity of 10^{12} Pa.s as obtained from viscosity fitting.

TABLE 1. Glasses tested in this study.

Glass	Chemical composition (mol%)						T_g (°C)	m	Average RMSD of $\log\eta, \eta$ in Pa.s	
	SiO_2	Al_2O_3	Na_2O	MgO	CaO	Other components			Shoving model	New model
MgAl0	75.83	0.07	15.63	8.11	0.19	-	512	29.7	0.30	0.02
MgAl8	68.07	7.99	15.71	7.98	0.09	-	618	31.5	0.40	0.06
MgAl16	59.92	15.98	15.77	8.08	0.09	-	700	33.2	0.35	0.03
MgAl24	52.02	23.97	15.82	7.93	0.09	-	739	38.6	0.49	0.04
CaAl0	75.88	0.03	15.72	0.10	8.11	-	531	35.6	0.45	0.05
CaAl8	68.08	8.02	15.72	0.09	7.92	-	594	35.3	0.34	0.04
CaAl16	59.83	16.01	15.79	0.13	8.08	-	678	35.2	0.45	0.04
CaAl24	51.82	23.97	15.81	0.13	8.11	-	765	39.8	0.51	0.06
Albite	75.00	12.50	12.50	0.00	0.00	-	812	25.6	0.27	0.03
Diopside	50.00	0.00	0.00	25.0	25.0	-	736	65.1	0.99	0.02
	Chemical composition (wt%)									
Cathedral glass[24]	53.26	1.0	2.9	7.11	12.81	17.12 K_2O, 4.4 P_2O_5, 1.2 MnO_2, 0.2 Fe_2O_3	586	38.8	0.39	0.05
NIST 710A[25]	67.55	2.10	8.05	0.00	8.50	9.30 K_2O, 3.60 ZnO,	547	30.3	0.39	0.11

						0.40 TiO_2, 0.05 As_2O_3, 0.20 Sb_2O_3				
NBS 710[26]	70.5		8.7		11.6	7.7 K_2O, 1.1 Sb_2O_3, 0.2 SO_3, 0.2 R_2O_3 (Fe_2O_3-0.02)	550	33.9	0.57	0.04
EAGLE XG	-						735	31.6	0.69	0.04
Jade Glass	-						792	35	0.37	0.06

Brillouin light scattering (BLS) experiments based on an emulated platelet geometry (EPG) were conducted to measure high-temperature elastic properties; further details of the experimental setup can be found in our previous work.[27] A Verdi V2 DPSS 532.18 nm green laser was used as the probing light source and a six-pass high-contrast Fabry–Perot interferometer from JSR Scientific Instruments was used to analyze the scattered light. To monitor the evolution of elastic properties as a function of temperature, BLS measurements were taken through the top fused quartz window of a Linkam TS1500 heating stage. Glasses were heated from room temperature to temperatures above their glass transition temperatures (T_g) for each composition with a heating rate of 50 °C/min. After the temperature inside the heating stage was stabilized for 5 min, Brillouin spectra were collected. BLS measurements in the EPG setup allows the measurement of both longitudinal (V_L) and transverse sound (V_T) velocities at high temperatures. From the sound velocities measured in BLS, together with the sample density (ρ), the Young's modulus (E), bulk modulus (B), shear modulus (μ), and the Poisson's ratio (v) can be calculated using

$$C_{11} = \rho V_L^2, \tag{3}$$

$$C_{44} = \rho V_T^2, \tag{4}$$

$$E = C_{44}\frac{3C_{11} - 4C_{44}}{C_{11} - C_{44}}, \tag{5}$$

$$B = \frac{3C_{11} - 4C_{44}}{3}, \tag{6}$$

$$\mu = C_{44}, \tag{7}$$

and

$$\nu = \frac{E}{2\mu} - 1. \tag{8}$$

The temperature dependence of equilibrium viscosity of the eight sodium alkaline-earth aluminosilicate glasses[4], diopside glass, cathedral glass[24], EAGLE XG[3] and Jade glass[4] were measured by performing beam bending, parallel plate, and concentric cylinder experiments.[28] The equilibrium viscosity of albite was obtained from literature[29]. The equilibrium viscosity of NIST 710A and NBS 710 were taken from the certificates published by the National Institute of Standards and Technology (NIST)[25] and the National Bureau of Standards (NBS)[26], respectively. In addition, isothermal equilibrium viscosity measurements[24] were conducted in the vicinity of the glass transition range to obtain the fragility index and T_g values of NIST 710A glass using Angell's fragility plot.[24,30]

III. MODEL DERIVATION

The activation barrier to viscous flow, $\Delta G_a(T)$, is defined by

$$\ln\left(\frac{\eta(T)}{\eta_\infty}\right) = \frac{\Delta G_a(T)}{k_B T}. \tag{9}$$

According to the shoving model in Eq.(1), the activation barrier to viscous flow is

$$\Delta G_a(T) = \mu_\infty(T) V_c, \tag{10}$$

implying that the non-Arrhenius behavior arises solely due to the temperature dependence of instantaneous shear modulus in the activation barrier.

We calculate V_c using Eq.(1) from experimental viscosity and high-frequency shear modulus values assuming validity of the shoving model at each temperature and show them in Fig. 1, which clearly shows that V_c is a temperature-dependent quantity, increasing with decreasing temperature, in good agreement with the Adam-Gibbs (AG) model[8], the random first-order transition (RFOT) theory[31] and the elastically collective nonlinear Langevin equation (ECNLE) theory[32]. Accounting for the temperature dependence of V_c in Eq.(10) gives

$$\Delta G_a(T) = \mu_\infty(T) V_c(T). \tag{11}$$

The functional form of $V_c(T)$ is not known. Based on the data of Fig. 1 we adopt the form

$$V_c(T) = V_\infty \exp\left(\frac{C}{T}\right) \tag{12}$$

where C is a fitting parameter that is later shown to be expressible in terms of other model parameters. The above functional form is very similar to that of the temperature-dependent

configurational entropy used in the MYEGA model[28], which is based on the energy landscape and temperature-dependent constraint theory. Furthermore, on comparing Fig. 1 with the temperature-dependent excess entropy[33], a possible inverse relationship between $V_c(T)$ and excess entropy is revealed.[8,28] It is known that excess entropy is not the same as configurational entropy; it has both vibrational and configurational contributions.[33] But it is generally agreed upon that excess entropy in the liquid regime is proportional to configurational entropy.[33] The above observations show that V_c and configurational entropy seem to be fundamentally linked, and V_c should not be assumed to be temperature independent as in the shoving model. Eq.(12) assumes that V_c changes with temperature, similar to the evolution of co-operatively rearranging units with temperature in the AG model. Eq.(11) indicates that both elasticity and configurational entropy contribute to the activation energy for temperature dependence viscosity.

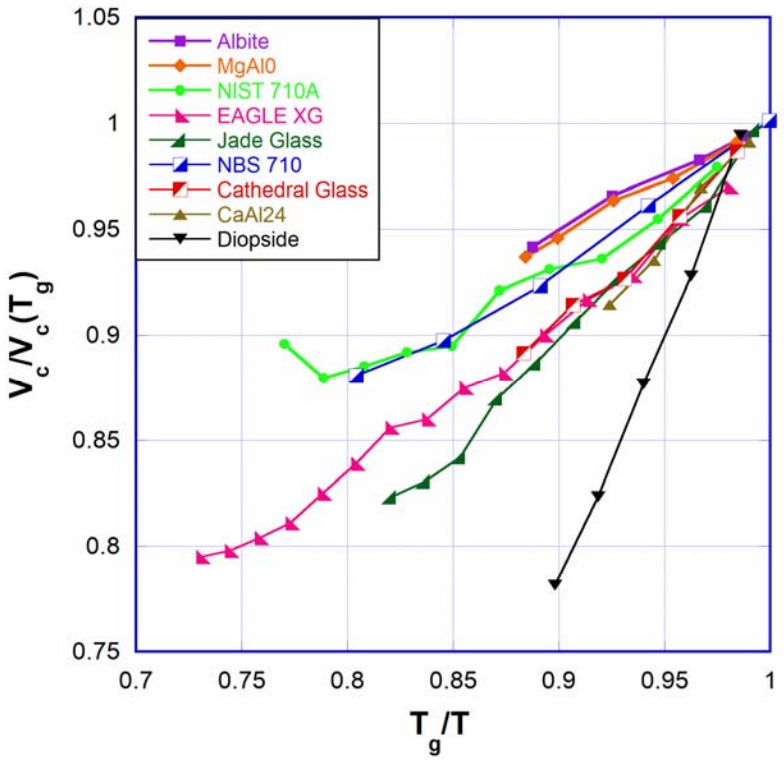

FIG. 1. Temperature dependence of characteristic volume (V_c) for glasses studied in this work.

Adopting the functional form for $V_c(T)$ as described in Eq.(12), we write the activation barrier for our new model as

$$\Delta G_a(T) = \mu_\infty(T) V_c(T) = \mu_\infty(T) V_\infty \exp(\frac{C}{T}) = \Delta G_a(T_g) \frac{\mu_\infty(T)}{\mu_\infty(T_g)} \exp(\frac{C}{T} - \frac{C}{T_g}). \quad (13)$$

The last expression in Eq.(13) uses Eq.(11) and Eq.(12), both evaluated at T=T_g, to obtain the relation

$$V_\infty = V_c(T_g)\exp(-\frac{C}{T_g}) = \frac{\Delta G_a(T_g)}{\mu_\infty(T_g)}\exp(-\frac{C}{T_g}) \tag{14}$$

used to reach the last equality in Eq.(13).

Using viscosity Eq.(9) and activation barrier Eq.(13), we write

$$\ln\frac{\eta(T)}{\eta_g} = \ln\frac{\eta(T)}{\eta_\infty} - \ln\frac{\eta_g}{\eta_\infty} = \frac{\Delta G_a(T)}{k_B T} - \frac{\Delta G_a(T_g)}{k_B T_g} = \frac{\Delta G_a(T_g)}{k_B T_g}\left[\frac{T_g}{T}\frac{\mu_\infty(T)}{\mu_\infty(T_g)}\exp(\frac{C}{T}-\frac{C}{T_g})-1\right] \tag{15}$$

where η_g is the viscosity at T_g which is 10^{12} Pa·s. Any equation describing the viscosity of glass-forming liquids in the equilibrium regime implies a value for fragility m, whose definition[34] is

$$m = \left.\frac{\partial \log_{10}\eta}{\partial\left(T_g/T\right)}\right|_{T=T_g} = -\frac{1}{\ln 10}\left.\frac{\partial \ln\eta}{\partial \ln T}\right|_{T=T_g}. \tag{16}$$

Differentiating viscosity Eq.(15) and evaluating at $T=T_g$ we get

$$\left(\frac{\partial \ln\eta(T)}{\partial \ln T}\right)_{T=T_g} = \frac{\Delta G_a(T_g)}{k_B T_g}\left[-1+\left(\frac{\partial \ln\mu_\infty(T)}{\partial \ln T}\right)_{T=T_g} - \frac{C}{T_g}\right]. \tag{17}$$

We combine Eq.(16) and (17) to solve for

$$\Delta G_a(T_g) = \frac{\ln 10\, m k_B T_g}{\left(1-\left.\frac{\partial \ln\mu_\infty(T)}{\partial \ln T}\right|_{T_g} + \frac{C}{T_g}\right)}. \tag{18}$$

The use of viscosity Eq.(15) along with activation barrier Eq.(18) gives

$$\log_{10}\frac{\eta(T)}{\eta_g} = \frac{m}{\left(1-\left.\frac{\partial \ln\mu_\infty(T)}{\partial \ln T}\right|_{T_g} + \frac{C}{T_g}\right)}\left[\frac{T_g}{T}\frac{\mu_\infty(T)}{\mu_\infty(T_g)}\exp\left(\frac{C}{T_g}\left(\frac{T_g}{T}-1\right)\right)-1\right]. \tag{19}$$

On taking $T\to\infty$, the first term in brackets vanishes and we are left with

$$\log_{10}\left(\frac{\eta(T\to\infty)}{\eta_g}\right) = -\left(\frac{m}{1-\left.\frac{\partial \ln\mu_\infty(T)}{\partial \ln T}\right|_{T=T_g} + \frac{C}{T_g}}\right) = \log_{10}\left(\frac{\eta_\infty}{\eta_g}\right). \tag{20}$$

It makes no difference whether we consider C or η_∞ as a fitting parameter as they are related by Eq.(20). Since most of viscosity models use η_∞, we solve Eq.(20) to get C in terms of η_∞ and then get rid of C completely from Eq.(19) to reach the final expression for the new model:

$$\log_{10}\left(\frac{\eta(T)}{\eta_g}\right)=\log_{10}\left(\frac{\eta_\infty}{\eta_g}\right)\left[1-\frac{T_g}{T}\frac{\mu_\infty(T)}{\mu_\infty(T_g)}\exp\left(\left[-\frac{m}{\log_{10}\left(\frac{\eta_\infty}{\eta_g}\right)}+\left.\frac{\partial\ln\mu_\infty(T)}{\partial\ln T}\right|_{T=T_g}-1\right]\left(\frac{T_g}{T}-1\right)\right)\right]. \quad (21)$$

Eq.(21) satisfies the correct values at $T=T_g$ and $T\to\infty$ and uses the fragility parameter m. This new model is a three-parameter model just like the VFT[35–37] or the MYEGA[28] model. The three parameters, η_∞, T_g, and m are meaningful physical properties for glass formers. The new model is an improvement over the shoving model in the equilibrium regime because it considers the contributions of both temperature-dependent shear modulus as well as characteristic volume (thus entropy) to explain the non-Arrhenius temperature dependence of viscosity.

It was recently[38] shown that the high-temperature viscosity limit (η_∞) of silicate liquids has a universal value of $10^{-2.93}$ Pa·s. Fragility index (m) and glass transition temperature (T_g) would be the only two fitting parameters in Eq.(21) in the equilibrium viscosity regime. m and T_g values so obtained for the glasses tested in this work are presented in Table 1 and these numbers were found to closely agree with those obtained by other methods/fits.[3,4,19,24,29]

This new elastic model can be extended to the glassy regime with a simple modification. We adopt the traditional view that structural arrest near the fictive temperature causes the configurational entropy of the glass to freeze at the same value as the liquid state just prior to the onset of glass transition.[39] In other words, we assume that in the glassy state, the configurational entropy change is minimal[22,33], and V_c is a constant and equal to $V_c(T_f)$ when $T<T_f$. The model will then be reduced in the non-equilibrium isostructural regime to

$$\ln\left(\frac{\eta(T,T_f)}{\eta_\infty}\right)=\frac{\mu_\infty(T,T_f)V_c(T_f)}{k_BT}. \quad (22)$$

Isostructural viscosity describes the viscosity of the glassy state based on the liquid structure from which it is frozen.[40] It refers to 'zero aging time' viscosity when the structure that is quenched-in from the fictive temperature has no time to relax.[41] The viscosity curves in Eq.(21) and Eq.(22) meet at T_f. On equating $\eta(T_f)$ from Eq.(21) and Eq.(22), we get $V_c(T_f)$. This $V_c(T_f)$ is then used in Eq.(22) to generate the entire non-equilibrium isostructural viscosity curve given the temperature-dependent shear modulus of a glass with a thermal history defined by T_f. Eq.(22) implies that glass viscosity is largely dependent on glass elasticity and $V_c(T_f)$; the latter is in turn determined by the dynamics of liquid.

IV. RESULTS

The high temperature elastic properties of all the glasses in this study were measured by the BLS technique described in Section II. Temperature-dependent BLS spectra are shown for a NIST 710A glass in Fig. 2(a) as an example. Fig 2(b) shows the high temperature shear modulus

of NIST 710A glasses of different thermal histories calculated from the BLS spectra. When the temperature of a glass is increased, near the glass transition range, a sharp change in the slope of the shear modulus is observed. As is evident from Fig. 2(b), thermal history affects only the properties of the glass but not those of the equilibrium liquid. Fig. 2(c) shows $V_c(T)$ adopted by the present model where an exponential form is taken for $T>T_f$ and a constant V_c is assumed for $T<T_f$.

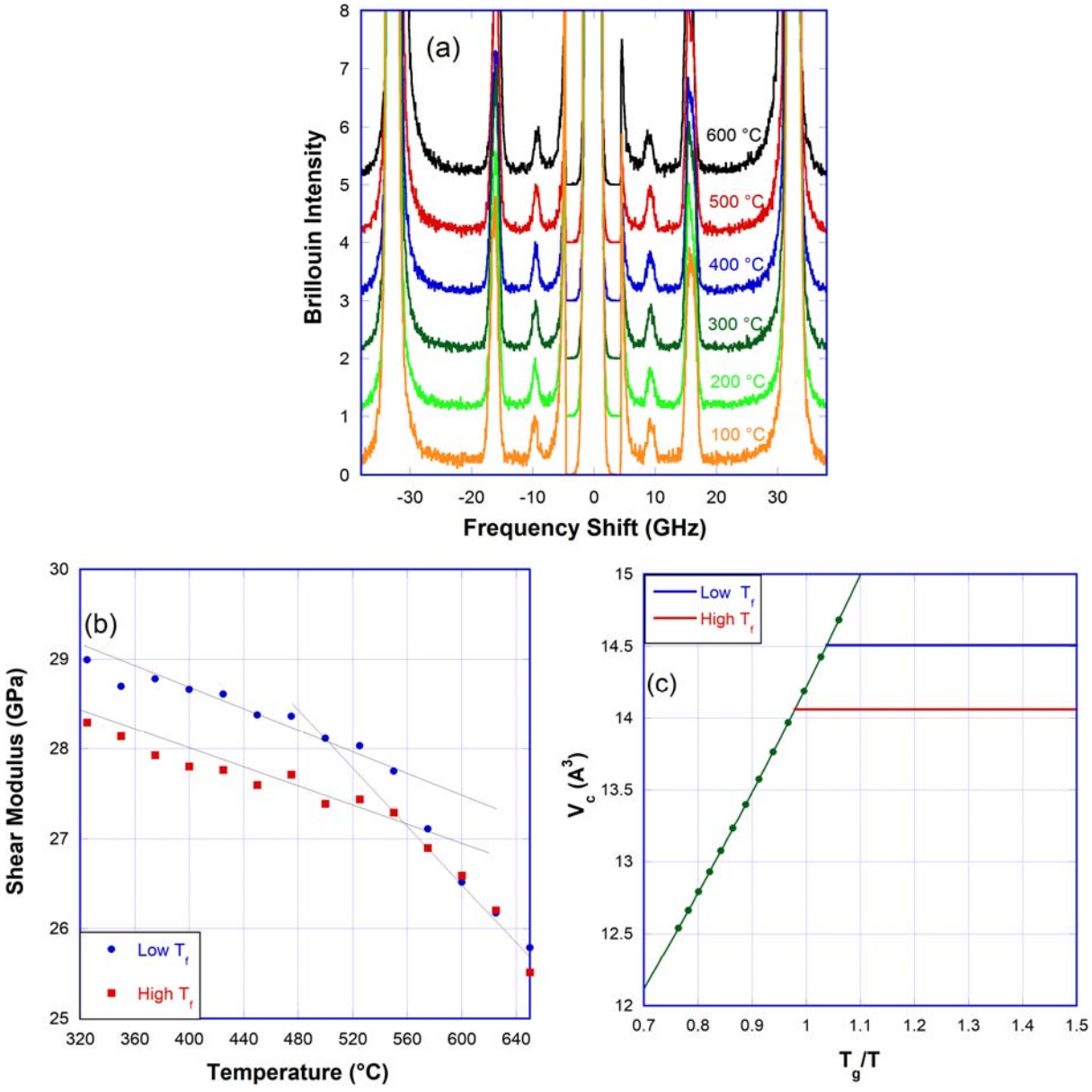

FIG. 2. (a) Brillouin spectra as a function of temperature from the EPG set-up for NIST 710A glass with high T_f, where the outer pair of peaks is from the Stoke's and anti-Stoke's scattering of longitudinal wave from the back scattering geometry, the middle and inner pair of peaks are from the longitudinal and shear waves from the platelet scattering geometry. Note: spectra are

shifted vertically as function of temperature for clarity. (b) High temperature elastic properties of NIST 710A with high and low T_f, and (c) temperature-dependent characteristic volume used in the new model.

The equilibrium viscosity in this work is represented by the MYEGA fit to experimentally-measured viscosity, as this model has been shown to fit fairly well to the equilibrium viscosity.[4,28] An example of the quality of fitting and the corresponding experimental data are shown for the standard NBS 710 glass[26] in Fig. 3. Equilibrium viscosity values from the MYEGA model were taken at temperatures where shear modulus was measured to fit both the new model and the shoving model. With a knowledge of equilibrium viscosity and high-temperature elasticity, the non-equilibrium isostructural viscosity can be predicted by following the procedure described in Section III. Figures 4 and 5 show the fitting to the equilibrium viscosity by the new model in comparison to the shoving model for strong liquids and fragile liquids. The non-equilibrium isostructural viscosity values are also included in Figs. 4 and 5.

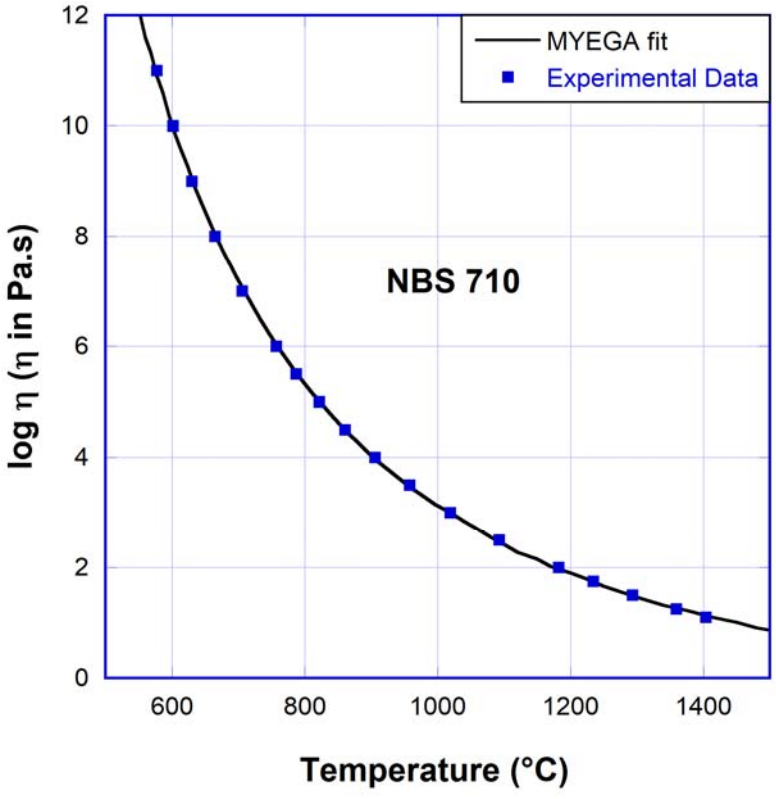

FIG. 3. Viscosity as a function of temperature for NBS 710 glass[26]. The data are fit with the MYEGA model.

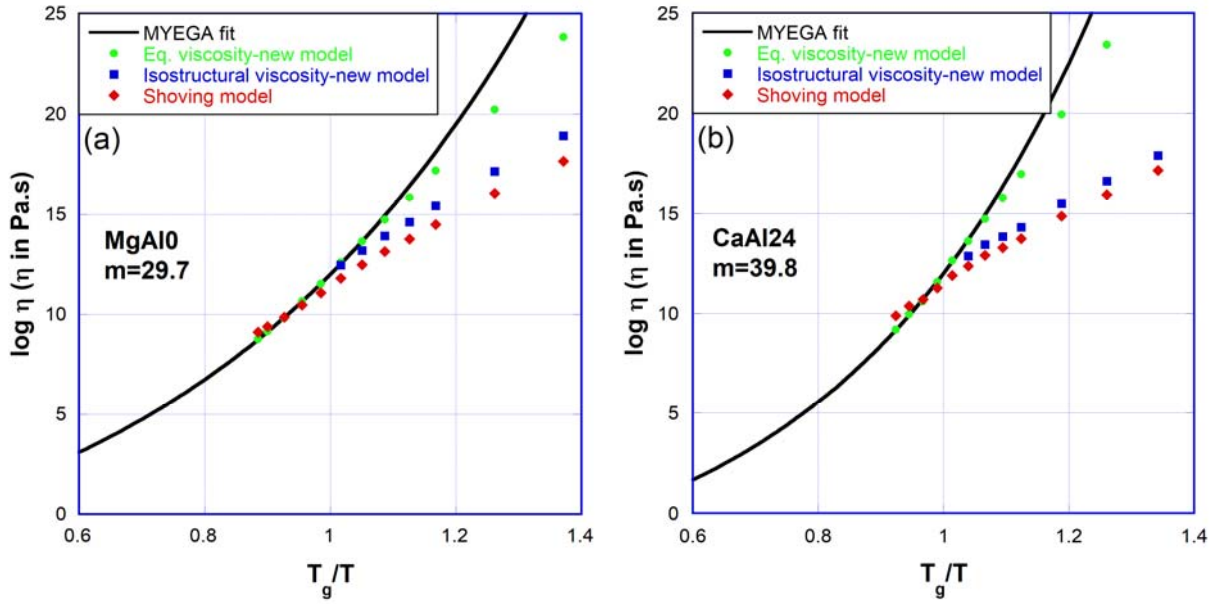

FIG. 4. Equilibrium and non-equilibrium isostructural viscosity predicted by the new model and the shoving model for (a) MgAl0 glass and (b) CaAl24 glass with different fragility.

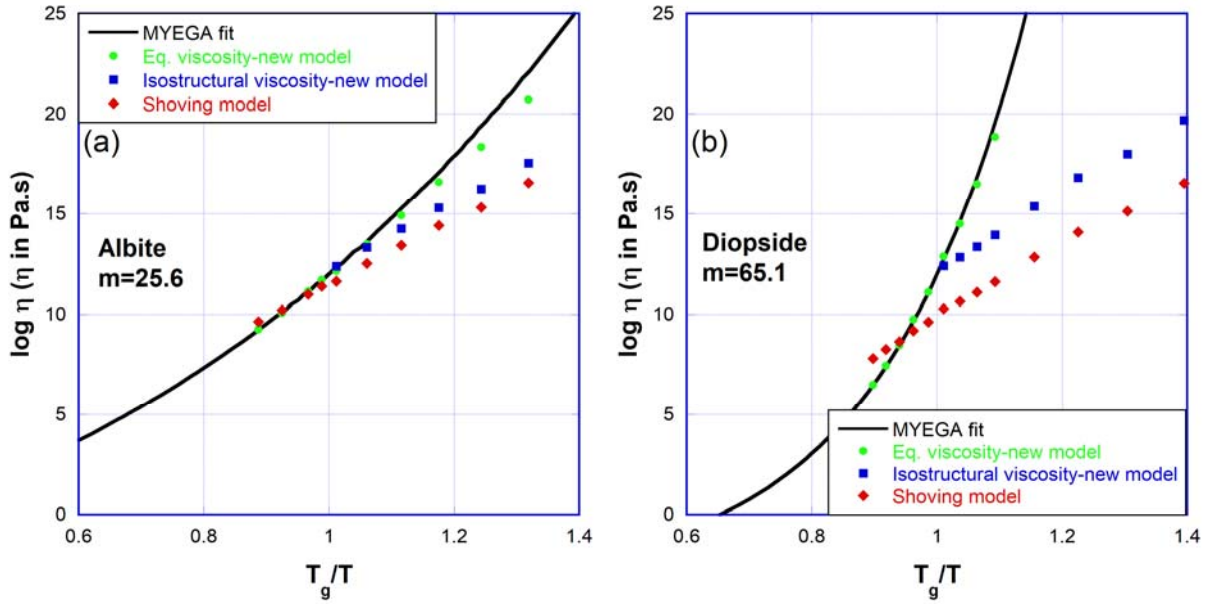

FIG. 5. Equilibrium and non-equilibrium isostructural viscosity predicted by the new model and the shoving model for (a) strong albite glass[29] and (b) fragile diopside glass.

The above results show that the new model works much better than the shoving model in fitting the equilibrium viscosity. Table 1 compares the average root mean square deviation

(RMSD) in the equilibrium viscosity predicted by the shoving model and the new model. It shows that the RMSDs of the new elastic model are much lower than those of the shoving model for all the glasses studied here. Figures 4 and 5 clearly show that the shoving model seems to work well for strong glasses, but very poorly for fragile glasses such as diopside, while the new model works equally well for both strong and fragile systems.

The viscosity and relaxation properties of the glassy state were previously shown to be linked to the equilibrium property, fragility.[1,3] It was shown that fragile glasses experience a more sudden departure from equilibrium, i.e., a more sudden breakdown of ergodicity immediately below T_g.[3] From Fig. 4 and 5, it is evident that the expected trend of fragile glasses experiencing a more sudden departure from equilibrium in the glassy state compared to strong glasses is captured by the new model.

Next, we test our model on a modern commercial glass, Corning EAGLE XG and a medieval cathedral glass. The modified elastic model is compared against the shoving model for EAGLE XG for which shear modulus could be reliably measured to temperatures as high as T_g/T around 0.7. The new elastic model fits the equilibrium viscosity to high temperatures perfectly as seen in Fig. 6(a), whereas the shoving model predicts a less steep or a stronger viscosity curve than what was observed experimentally. Results for a medieval cathedral glass composition from Westminster Abbey dated 1268 AD[24] are shown in Fig. 6(b). The new model fits equilibrium viscosity better than the shoving model for this glass as well. Coincidentally, because $V_c(T_f$=633 °C) in our model matches with the V_c optimized from the shoving model, both give the same isostructural viscosity in the glassy state. The past two decades have seen a lot of interest on the viscous flow of such medieval glasses from European cathedrals in order to dismiss the popular legend that medieval glasses flow at room temperature[24,40,42] Our new model predicts the room temperature isostructural viscosity to be $10^{39.98}$ Pa.s , close to the value of $10^{41.3}$ Pa.s calculated by Zanotto and Gupta for a soda lime silicate glass.[40] Using the room temperature μ_∞ for this glass, 28.25 GPa, we find that the Maxwell relaxation time is 1.1×10^{22} years, which is much longer than the lifetime of the cathedrals, once again proving that the flow of cathedral glasses at room temperature is just a myth. A recent work based on the MAP model for non-equilibrium viscosity calculated a much lower viscosity for the same glass, $10^{24.6}$ Pa.s, which is about 15 orders of magnitude lower than these estimates.[24] It should be pointed out that the non-equilibrium viscosity described by the MAP model is different from the isostructural viscosity described here.[19]

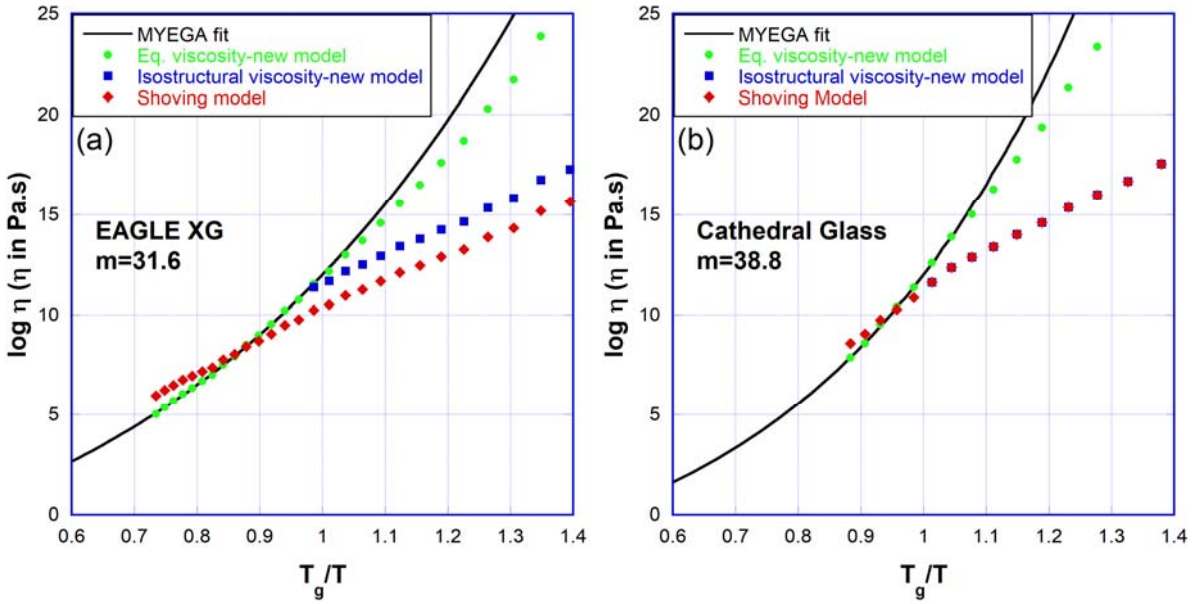

FIG. 6. Equilibrium and non-equilibrium isostructural viscosity predicted by the current model and the shoving model for (a) EAGLE XG (T_f=764.8 °C) and (b) cathedral glass (T_f=633.2 °C).

The VFT equation[35–37]

$$\eta(T) = \eta_\infty \exp\left[\frac{B}{T - T_0}\right] \tag{23}$$

was extended to the isostructural regime by Yue[22] as

$$\eta(T, T_f) = \eta_\infty \exp\left[\frac{BT_f}{T(T_f - T_0)}\right]. \tag{24}$$

On comparing the non-equilibrium isostructural viscosity predicted by our model against Yue's isostructural viscosity model[22] and against Mazurin's experimental measurements on a standard NBS 710 glass[17], we found excellent agreements as seen clearly in Fig. 7.

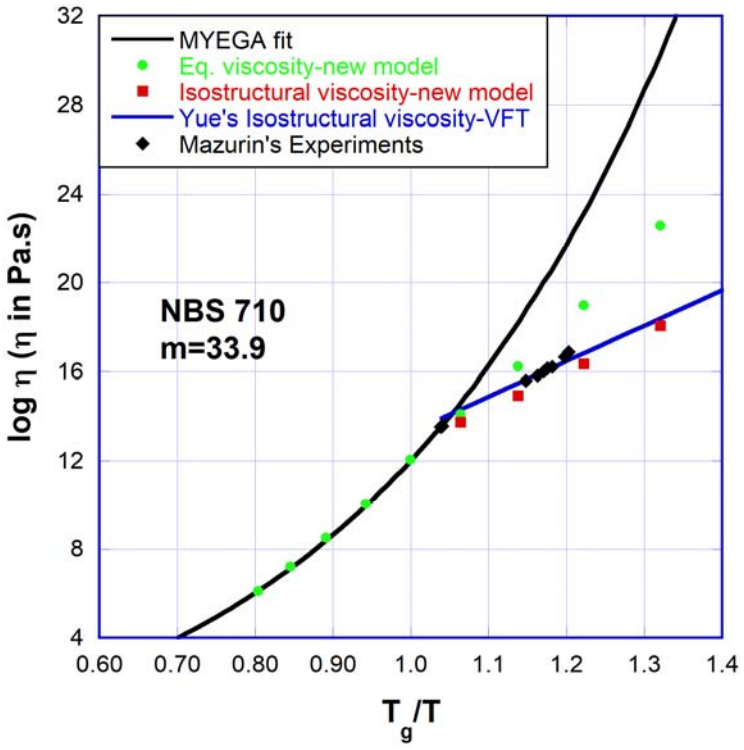

FIG. 7. Non-equilibrium isostructural viscosity predicted by the new model, Yue's model[22] and from experimental measurements[17] for NBS 710.

The modified elastic model was applied to glass samples of NIST 710 A and Corning Jade glass with different fictive temperatures and the results are represented in Fig. 8, which clearly shows that the new model successfully separates the isostructural viscosity of glasses based on their thermal history. These results show that a glass with a higher fictive temperature has a lower viscosity, in good agreement with previous studies on glass viscosity.[3,21,41]

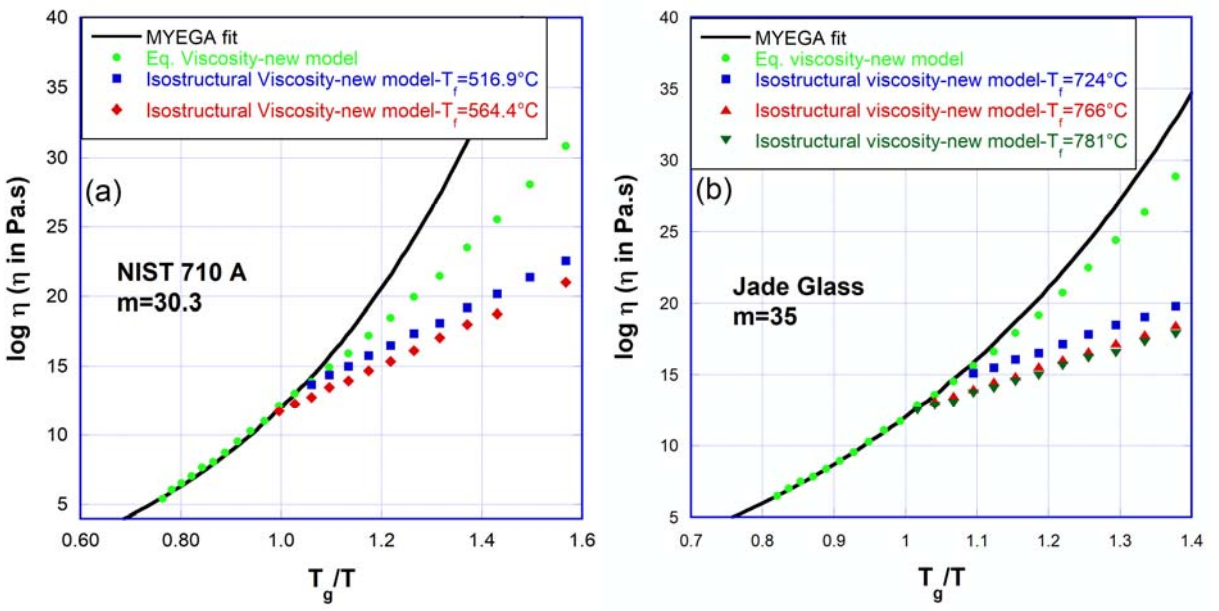

FIG. 8. Equilibrium and non-equilibrium isostructural viscosity predicted by the current model for (a) NIST 710 A glasses and (b) Jade glass with different thermal histories.

Figure 9 shows the variation of isostructural viscosity against fictive temperature of Jade glass at a constant temperature of 400 °C, i.e., T_g/T=1.58 (chosen just as an example). Viscosity changes by more than 2 orders of magnitude as fictive temperature changes about 60 °C in this viscosity/temperature range. A similar magnitude of viscosity variation with fictive temperature was reported previously using the MAP model on the same Jade glass.[21] According to the present model, the activation energy in the glassy state not only depends on the shear modulus, but also $V_c(T_f)$ as shown in Eq.(22). This was not considered in a previous work which extended the shoving model to the glassy regime according to Eq.(2).[21] Fig. 9 also includes viscosity values predicted by the shoving model using Eq.(2), which gives too small changes in glass viscosity with the change in T_f as V_c is kept constant.

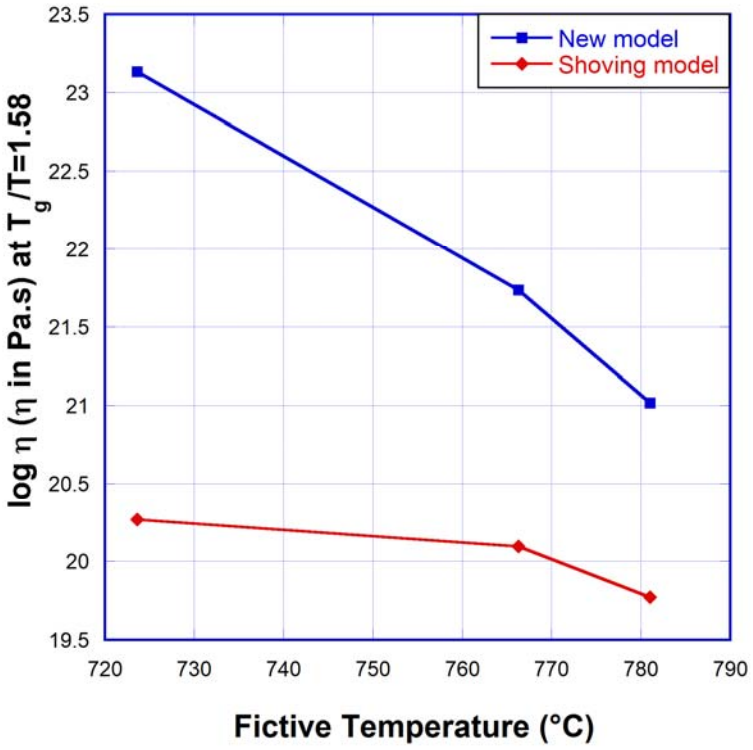

FIG. 9. Dependence of isostructural viscosity on fictive temperature of Jade glass at T_g/T=1.58.

V. DISCUSSION

A. Overcoming the limitations of the shoving model

Elastic models connect the short and long time scales via the following philosophy: relaxation is slow because the barriers to be overcome for a molecular rearrangement are large. The barrier transition itself, however, is a fast process which may well be determined by the system's short-time properties, for instance its elastic constants probed on the short time scale.[13] The energy barrier to be overcome for a molecular rearrangement is dominated by the elastic work done in 'shoving aside' the surrounding molecules, which is proportional to the short-time shear modulus. Several experiments were done to test the elastic models for viscosity like the shoving model to further the fundamental understanding of the origins of fragility and it was found that while some studies support the model[10,13,43], many others do not[4,44,45]. The temperature dependence of shear modulus alone was found to be insufficient to explain the non-Arrhenius temperature dependence of viscosity as discussed extensively in the Section IV.

The current modified elastic model has its physical basis in both the shoving model and the AG model. A flow event takes place by barrier transition of co-operatively rearranging units. We argue that the activation free energy for this flow event depends both on the barrier height as well as the size of the co-operatively rearranging units. The barrier transition happens on very short timescales and its height depends on the high-frequency shear modulus. The size of the co-

operatively rearranging units is temperature-dependent and related to the configurational entropy. Our model demonstrates that the non-Arrhenius temperature dependence of equilibrium viscosity is governed by both configurational entropy as well as elasticity. Thus, by incorporating the effect of configurational entropy, we overcome the limitations of the shoving model. The new model fits both strong and fragile glasses studied in this work equally well.

B. Success of the MYEGA model: role of shear modulus?

The MYEGA model is based on the Adam-Gibbs theory.[28] Its ability to fit the viscosity of a diverse set of glass-forming liquids may question the importance of the role of shear modulus in controlling viscosity. In this section, we will compare it with the modified elastic model and examine why the MYEGA model seemingly works well even though it does not take into account the temperature-dependent shear modulus.

The MYEGA viscosity model[28]

$$\log_{10}\eta(T)=\log_{10}\eta_\infty+\left(\log_{10}\eta_g-\log_{10}\eta_\infty\right)\frac{T_g}{T}\exp\left[\left(\frac{m}{\log_{10}\eta_g-\log_{10}\eta_\infty}-1\right)\left(\frac{T_g}{T}-1\right)\right] \quad (25)$$

can be rewritten in the form:

$$\log_{10}\frac{\eta(T)}{\eta_g}=\log_{10}\frac{\eta_\infty}{\eta_g}\left\{1-\frac{T_g}{T}\exp\left[\left(-\frac{m}{\log_{10}\frac{\eta_\infty}{\eta_g}}-1\right)\left(\frac{T_g}{T}-1\right)\right]\right\} \quad (26)$$

and compared with the new model in Eq.(21). This side by side comparison makes it clear that these two models agree when

$$\frac{\mu_\infty(T)}{\mu_\infty(T_g)}\exp\left[\left(-\frac{\partial\ln\mu_\infty(T)}{\partial(T_g/T)}\bigg|_{T=T_g}\right)\left(\frac{T_g}{T}-1\right)\right]=1 \quad (27)$$

or equivalently

$$\ln\mu_\infty(T)=\ln\mu_\infty(T_g)+\frac{\partial\ln\mu_\infty(T)}{\partial(T_g/T)}\bigg|_{T=T_g}\left(\frac{T_g}{T}-1\right). \quad (28)$$

This says when $\ln\mu_\infty(T)$ vs. T_g/T is a straight line, these two models agree. Indeed, an Arrhenius function seems to fit well for $\mu_\infty(T)$ vs. T_g/T for glasses studied in this work (some examples are shown in Fig. 10) and for those studied in the literature[10], implying a single activation barrier for $\mu_\infty(T)$. This may explain why models based on the Adam-Gibbs theory work well even though the importance of the shear modulus as a factor controlling viscosity was not considered. Therefore, the MYEGA model can be considered as a special case for the modified elastic viscosity model proposed here. In other words, the new model provides a

generalization of the MYEGA model regardless of how the instantaneous shear modulus changes with temperature. Furthermore, the new model can be easily extended into the non-equilibrium isostructural regime when temperature is below T_f by simply switching the V_c to a constant corresponding to the characteristic volume at T_f. $V_c(T_f)$ carries the information of liquid dynamics and most of the information of thermal history into the isostructural viscosity of glass ($\mu_\infty(T)$ of the glassy state is only weakly dependent on T_f).

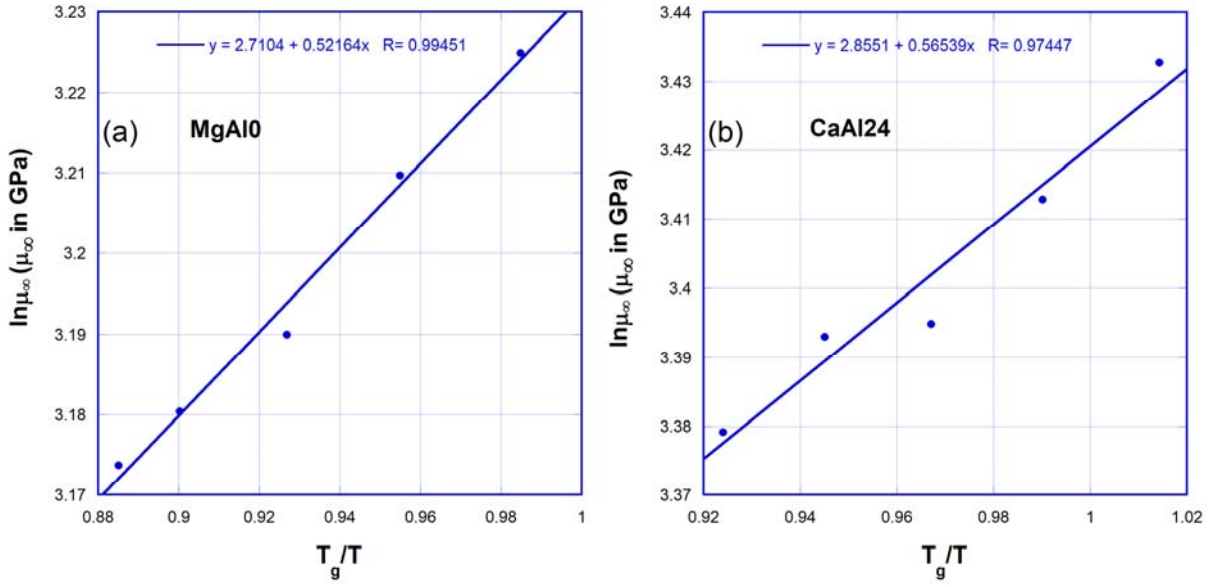

FIG. 10. Temperature dependence of instantenous shear modulus for (a) MgAl0 and (b) CaAl24.

C. Isostructural viscosity

Results in Section IV demonstrate that the new isostructural viscosity model is able to capture the difference in viscosity trends expected with varying fictive temperature and varying fragility. Also, the numerical values of isostructural viscosity predicted by the new model were shown to be in excellent agreement with experiments[17] and with Yue's isostructural viscosity model[22]. Activation enthalpy defined by $k\left(d\ln\eta / d(\frac{1}{T})\right)$ in the glassy state using Eq.(22) comes out to be $V_c(T_f)[\mu_\infty(T,T_f)+\frac{1}{T}\left(d(\mu_\infty(T,T_f) / d(\frac{1}{T})\right)]$. This quantity weakly increases with decreasing temperature for normal glasses revealing slightly non-Arrhenius behavior in the non-equilibrium

viscosity. This trend is in agreement with experiments[41] and a previous isostructural viscosity model.[41] Also, according to the new model, glasses with higher fictive temperatures have lower activation enthalpy because $V_c(T_f)$ decreases with increasing T_f. This trend is also in agreement with previous non-equilibrium viscosity models.[41]

The present model uses a single quantity, T_f, along with glassy state elasticity to calculate the isostructural viscosity. The model provided here is an important step forward which considers the temperature dependence of shear modulus of glass to be a significant factor contributing to the isostructural viscosity along with equilibrium viscosity parameters embodied in $V_c(T_f)$. This indicates that the viscosity of glass is closely linked to glass elasticity and liquid dynamics, which agrees with recent studies[19,22].

The current isostructural viscosity model and some previous isostructural viscosity calculations[22,40] in literature adopt the traditional view of configurational entropy frozen-in at T_f as opposed to the view that glass transition involves a gradual loss of configurational entropy.[39] The current model can be further improved with a full understanding of the temperature dependence of entropy in the glass transition range. If configurational entropy can be reliably measured in the glass transition, a functional form for its temperature dependence can be created. This will improve the isostructural form of the current model and will allow it to capture the gradual transition between the supercooled and glassy states. Advances in experiments and in theoretical understanding of entropy loss near glass transition and how it depends on fragility can meaningfully improve the current model. Alternatively, since it is very difficult to directly measure configurational entropy experimentally, reliable measurements of non-equilibrium viscosity and elasticity in the glass transition range can be used along with the new model to generate the temperature dependence of V_c, which in turn provides a way to understand the temperature dependence of configurational entropy.

VI. CONCLUSIONS

A modified elastic model was introduced to consider the impact of both configurational entropy and elasticity on viscosity. It shows better agreements with high-temperature viscosity compared to the shoving model in the equilibrium regime for both strong and fragile liquids. With a simple modification, the new model can be extended to the glassy regime. It successfully separates strong and fragile behavior in equilibrium and isostructural regimes and accounts for thermal history differences in the predicted isostructural viscosity. The new model also supports the recent finding that equilibrium melt dynamics is intimately linked to the dynamics of the glassy state.

ACKNOWLEDGEMENTS

This work was supported by National Science Foundation under grant no. DMR-1508410 and DMR-1255378. L. Huang would like to thank Corning Inc. for supporting part of this research during her sabbatical leave through the Gordon F. Fulcher Sabbatical Program. The authors acknowledge valuable discussions with Drs. Yuanzheng Yue and Morten Mattrup Smedskjær (Aalborg University), Tanguy Rouxel (Université of Rennes) and Yunfeng Shi (Rensselaer Polytechnic Institute). Ruofu Sun's help with elasticity measurements is very much appreciated.

REFERENCES

[1] J.C. Mauro, J. Non-Cryst. Solids **357**, 3520 (2011).
[2] P.K. Gupta and J.C. Mauro, Phys. Rev. E **78**, (2008).
[3] J.C. Mauro, D.C. Allan, and M. Potuzak, Phys. Rev. B **80**, 94204 (2009).
[4] M.M. Smedskjaer, L. Huang, G. Scannell, and J.C. Mauro, Phys. Rev. B **85**, 144203 (2012).
[5] S. Sastry, Nature **409**, 164 (2001).
[6] P.K. Gupta and J.C. Mauro, J. Chem. Phys. **130**, 94503 (2009).
[7] S. Sen, J. Chem. Phys. **137**, 164505 (2012).
[8] G. Adam and J.H. Gibbs, J. Chem. Phys. **43**, 139 (1965).
[9] J. Dyre, N.B. Olsen, and T.E. Christensen, Phys. Rev. B Condens. Matter Mater. Phys. **53**, 2171 (1996).
[10] T. Rouxel, J. Chem. Phys. **135**, 184501 (2011).
[11] B.A.P. Betancourt, P.Z. Hanakata, F.W. Starr, and J.F. Douglas, Proc. Natl. Acad. Sci. **112**, 2966 (2015).
[12] U. Buchenau, R. Zorn, and M.A. Ramos, Phys. Rev. E **90**, 42312 (2014).
[13] T. Hecksher and J.C. Dyre, J. Non-Cryst. Solids **407**, 14 (2015).
[14] J.C. Dyre and W.H. Wang, J. Chem. Phys. **136**, 224108 (2012).
[15] F. Puosi and D. Leporini, J. Chem. Phys. **136**, 41104 (2012).
[16] O. Narayanaswamy, J. Am. Ceram. Soc. **54**, 491 (1971).
[17] O.V. Mazurin, V.P. Kluyev, and S.V. Stolyar, Glas. Ber K **56**, 1148 (1983).
[18] I. Avramov, J. Chem. Phys. **95**, 4439 (1991).
[19] X. Guo, M.M. Smedskjaer, and J.C. Mauro, J. Phys. Chem. B (2016).
[20] Q. Zheng and J.C. Mauro, J. Am. Ceram. Soc. **100**, 6 (2017).
[21] M. Potuzak, X. Guo, M.M. Smedskjaer, and J.C. Mauro, J. Chem. Phys. **138**, 12A501 (2013).
[22] Y. Yue, J. Non-Cryst. Solids **355**, 737 (2009).
[23] X. Guo, M. Potuzak, J.C. Mauro, D.C. Allan, T.J. Kiczenski, and Y. Yue, J. Non-Cryst. Solids **357**, 3230 (2011).
[24] O. Gulbiten, J.C. Mauro, X. Guo, and O.N. Boratav, J. Am. Ceram. Soc. **101**, 5 (2018).
[25] *Standard Reference Material 710A, Soda-Lime-Silica Glass* (National Institute of Standards & Technology, Gaithersburg, MD, USA, 1991).
[26] *Standard Sample No. 710, Soda-Lime-Silica Glass* (National Bureau of Standards, Washington, D.C., USA, 1962).
[27] M. Guerette and L. Huang, J. Phys. Appl. Phys. **45**, 275302 (2012).

[28] J.C. Mauro, Y. Yue, A.J. Ellison, P.K. Gupta, and D.C. Allan, Proc. Natl. Acad. Sci. **106**, 19780 (2009).
[29] A. Sipp, Y. Bottinga, and P. Richet, J. Non-Cryst. Solids **288**, 166 (2001).
[30] G. Yang, O. Gulbiten, Y. Gueguen, B. Bureau, J.-C. Sangleboeuf, C. Roiland, E.A. King, and P. Lucas, Phys. Rev. B **85**, 144107 (2012).
[31] V. Lubchenko and P.G. Wolynes, Annu Rev Phys Chem **58**, 235 (2007).
[32] S. Mirigian and K.S. Schweizer, J. Chem. Phys. **140**, 194506 (2014).
[33] L.-M. Martinez and C.A. Angell, Nature **410**, 663 (2001).
[34] C.A. Angell, Relax. Complex Syst. **22161**, 3 (1985).
[35] H. Vogel, Phys Z **22**, 645 (1921).
[36] G.S. Fulcher, J. Am. Ceram. Soc. **8**, 339 (1925).
[37] G. Tammann and W. Hesse, Z. Für Anorg. Allg. Chem. **156**, 245 (1926).
[38] Q. Zheng, J.C. Mauro, A.J. Ellison, M. Potuzak, and Y. Yue, Phys. Rev. B **83**, 212202 (2011).
[39] J.C. Mauro, R.J. Loucks, and S. Sen, J. Chem. Phys. **133**, 164503 (2010).
[40] E.D. Zanotto and P.K. Gupta, Am. J. Phys. **67**, 260 (1999).
[41] P.K. Gupta and A. Heuer, J. Non-Cryst. Solids **358**, 3551 (2012).
[42] E.D. Zanotto, Am. J. Phys. **66**, 392 (1998).
[43] M. Ikeda and M. Aniya, J. Non-Cryst. Solids **431**, 52 (2016).
[44] U. Buchenau, Phys. Rev. B **80**, (2009).
[45] L. Larini, A. Ottochian, C. De Michele, and D. Leporini, Nat. Phys. **4**, 42 (2008).